

Special Section:

Forum for Arctic Modeling and
Observational Synthesis (FAMOS)
2: Beaufort Gyre phenomenon

Key Points:

- Arctic double-diffusive staircases and intrusions have along-layer temperature/salinity gradients that arise from vertical flux divergences
- The transition in depth between staircases and intrusions depends on basin-scale lateral temperature gradients and stratification strength
- The magnitude of lateral Atlantic Layer heat and salt transport depends on vertical stratification and distance from the boundary current

Correspondence to:

Y. Bebieva,
yana.bebieva@yale.edu

Citation:

Bebieva, Y., & Timmermans, M.-L. (2019). Double-diffusive layering in the Canada Basin: An explanation of along-layer temperature and salinity gradients. *Journal of Geophysical Research: Oceans*, 124. <https://doi.org/10.1029/2018JC014368>

Received 20 JUL 2018

Accepted 1 JAN 2019

Accepted article online 6 JAN 2019

Double-Diffusive Layering in the Canada Basin: An Explanation of Along-Layer Temperature and Salinity Gradients

Yana Bebieva¹ and Mary-Louise Timmermans¹

Department of Geology and Geophysics, Yale University, New Haven, CT, USA

Abstract Double-diffusive mixing gives rise to layered structures in the Arctic Ocean: layers within a double-diffusive staircase overlying deeper layers associated with thermohaline intrusions. These layers exhibit well-defined lateral temperature and salinity gradients. Gradients in salinity along individual layers change sign with depth, while along-layer gradients in temperature remain the same sign with depth. A theoretical formalism is put forward to explain these features in terms of vertical divergences of double-diffusive fluxes; temperature and salinity gradients along layers are set by the depth-dependent ratio of double-diffusive heat to salt fluxes. Examination of fine structure in temperature and salinity profiles reveals how the net flux ratio depends upon whether the layer is part of an evolving thermohaline intrusion or a staircase. The physical framework in context with observations of varying along-layer gradients in temperature and salinity provides evidence for thermohaline intrusions evolving to a staircase and describes the parameters that dictate this process. Results bring new understanding to heat and salt transport in the Arctic Ocean as well as the physics of double-diffusive layering in the world's oceans.

Plain Language Summary A type of ocean mixing process, double-diffusive convection, gives rise to layers in the Arctic Ocean that may be characterized by their differing temperature and salinity properties. The properties and physics of these layers are key to understanding how heat is transported vertically and laterally in the Arctic Ocean. A theoretical formalism is put forward to explain distinct features of the layers that are characterized in the observations. The physical framework in context with observations brings new understanding to how the layers evolve and how they relate to heat and salt transport in the Arctic Ocean.

1. Introduction

The distribution and transport of heat in the Arctic Ocean are essential elements of the Arctic climate system. In the Arctic's central Canada Basin, warm and salty water originating from the Atlantic Ocean underlies colder and fresher water layers. The corresponding vertical stratification, with both temperature and salinity increasing with depth (while density is stably stratified), is amenable to double-diffusive convection (DC), one of the two types of double-diffusive mixing. A double-diffusive staircase in the region has been the subject of a number of studies (e.g., Neshyba et al., 1971; Neal & Neshyba, 1973; Padman & Dillon, 1987; Perkin & Lewis, 1984; Timmermans et al., 2008). Layers in the staircase range in thickness from 2 to 5 m; these mixed layers are separated by thin interfaces around 10 cm in thickness across which temperature and salinity increase sharply by ~ 0.04 °C and 0.014, respectively (Figures 1a and 1b). Individual layers within the staircase are laterally coherent over hundreds of kilometers across the Canada Basin, as evidenced in potential temperature (θ)-salinity (S) space where mixed layer properties group along lines (forming clusters; Figure 2). The slope of these lines reveals the magnitude of θ and S gradients along layers. It has been argued that these gradients arise from a balance between advection of properties along the layers and vertical divergences of double-diffusive temperature and salt fluxes (Timmermans et al., 2008).

The other type of double-diffusive mixing (termed salt finger, SF) occurs when both θ and S have vertical profiles that decrease with depth, while density is stably stratified. The SF type of double diffusion can be observed below the DC staircase in the depth region of the Atlantic water (AW) temperature maximum (Figure 1). Thermohaline intrusions, characterized by SF and DC regions alternating in depth, are often prominent in this portion of the water column (e.g., Bebieva & Timmermans, 2016; Carmack et al., 1998;

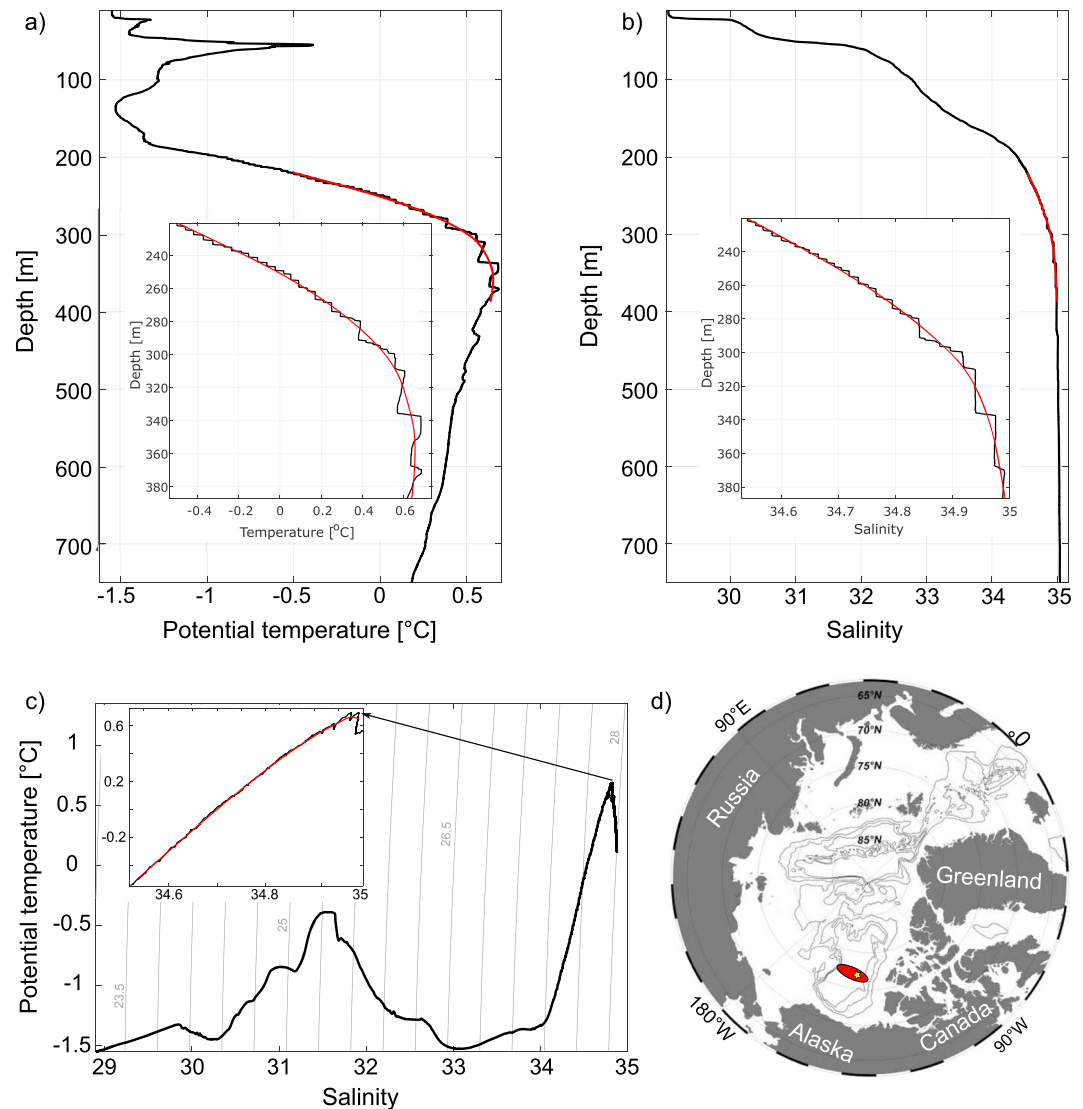


Figure 1. (a) Potential temperature ($^{\circ}\text{C}$, referenced to the surface) and (b) salinity profiles from ITP 2 on 7 September 2004 at the location of the yellow star on the map in panel d, and (c) the corresponding potential temperature-salinity profile with thin gray contours indicating potential density anomaly (kg/m^3) referenced to the surface. Insets show the closeup structures between ~ 220 - and ~ 380 -m depth, and red lines are the cubic spline fits to the profiles (see text). (d) Map showing the region of the Canada Basin where ITP 1 and ITP 2 were operating. ITP = Ice-Tethered Profiler.

McLaughlin et al., 2004). Lateral coherence is a feature of the intrusions as well, with SF regions of intrusions forming nested structures and organizing along lines (clusters) in θ - S space (Walsh & Carmack, 2003). The vertical gradients within an SF portion of intrusions are “mapped” into the along-layer gradients, which has been explained as the manifestation of slant-wise convection within an SF gradient; the colder and fresher part of an intrusion upstream mixes laterally with the warmer and saltier part of the intrusion downstream (see Figure 8 in Walsh & Carmack, 2003). While both the staircase and thermohaline intrusions exhibit along-layer gradients and coherency in θ - S space (Figure 2), their relationship to each other remains unclear. Understanding this relationship is a central aim of this paper.

This paper is motivated by observations, described in the next section, that suggest a distinct relationship between the DC staircase and thermohaline intrusions in the Canada Basin. In particular, we aim to explain why gradients in θ and S along staircase mixed layers and intrusions show a specific variation with depth. We reveal how interpreting these unmistakable characteristics of double diffusion in the Arctic Ocean sheds new light on their physical mechanisms and associated heat and salt fluxes. In section 3 we formulate a

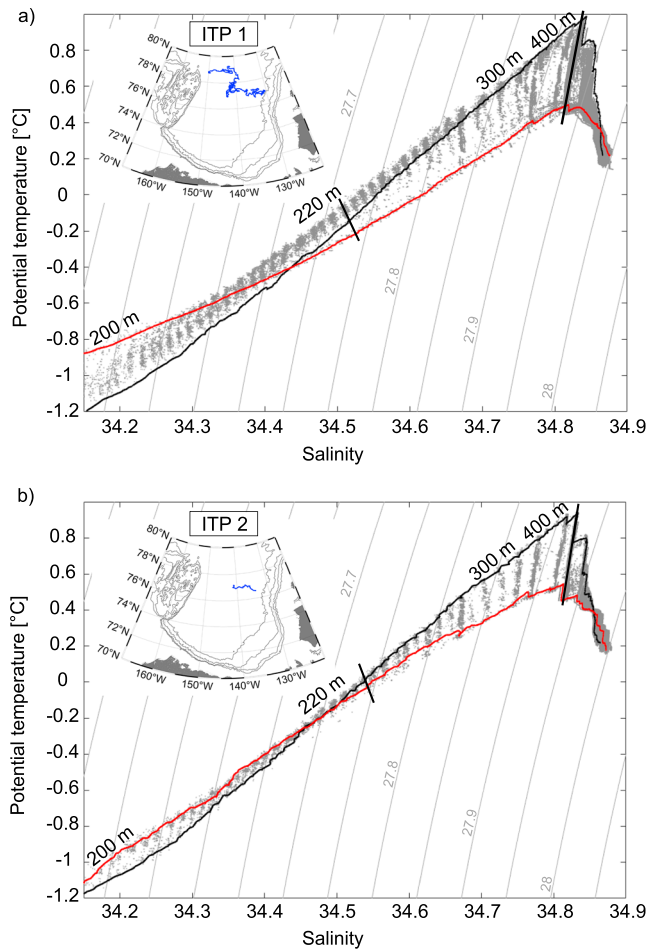


Figure 2. Potential temperature and salinity values measured by (a) ITP 1 and (b) ITP 2 between ~200- and ~750-m depth (gray dots, all profiles are shown). Black and red lines represent bounding profiles from the western and eastern extents of the drift tracks, respectively. Thin gray contours indicate lines of constant potential density anomaly (kg/m^3) referenced to the surface. Straight black lines show examples of the cluster slopes, and approximate water column depths are labeled. Map insets show a zoomed-in region of Figure 1d and ITP drift tracks from west to east (blue). ITP = Ice-Tethered Profiler.

theoretical model describing the variation of $\theta - S$ properties along staircase layers and intrusions that depends on the ratio of vertical fluxes of salt and heat. Section 4 sets the observations in context with the theoretical model to show how the flux ratio and heat and salt fluxes change with depth through the Canada Basin staircase and intrusions and how these relate to along-layer property gradients. Section 5 interprets the results in terms of the fine-scale observations, and section 6 draws on the findings to outline the underlying reason for the transition in depth from a staircase to intrusions. We summarize our study in section 7.

2. Observations

Seawater property data analyzed here are from Ice-Tethered Profilers (ITPs) that drifted in the Canada Basin (Krishfield et al., 2008; Toole et al., 2011). The ITP is an autonomous system that consists of a buoy mounted in the sea ice cover and a tether suspended below that supports a profiling unit. The CTD on the profiling unit returns temperature, conductivity (to infer salinity), and pressure measurements from around 7-m depth through the AW layer down to ~750-m depth with accuracies of ± 0.001 °C, ± 0.005 , and ± 1 dbar, respectively. Data have a vertical resolution of about 25 cm, and horizontal resolution between profiles is typically around 2 km depending on ice drift speed. The fully processed ITP data are analyzed here (data are available at www.whoi.edu/itp, and processing details are given by Krishfield et al., 2008). We analyzed approximately 2,000 profiles from ITP 1 operating between 16 August 2005 and 8 January 2007 and 240 profiles from ITP 2 operating between 20 August 2004 and 29 September 2004 in the region of the Canada Basin shown in Figure 1d.

ITP observations show distinct $\theta - S$ relationships characterizing the double-diffusive staircases and intrusions in the Canada Basin. Following the double-diffusive structures laterally along the ITP drift region from the western to the eastern side of the basin, ITP temperature and salinity profiles reveal that staircase mixed layers and SF regions of intrusions cluster along lines in $\theta - S$ space (Figure 2). Each cluster, which represents either a DC mixed layer or the SF portion of an intrusion (throughout the paper we will also refer to the SF portion of a thermohaline intrusion as a layer), has a well-defined slope, where this slope varies with depth (i.e., along-layer θ and S gradients change from one layer to the next). On average θ decreases and S increases from west to east along the layers in the shallow portion of the water column where layers are predominantly mixed layers in a DC staircase. In the deeper region, characterized by intrusions, both θ and S decrease from west to east along a layer (Figure 2). Thus, the cluster slope in $\theta - S$ space changes with depth from negative values at shallow depths to positive values in the deeper portion.

Detailed analysis of the fine structures in ITP profiles indicates that the sign of the cluster slope correlates well with whether a staircase or intrusion is observed. To show this correlation, we compute a fine-scale vertical gradient of potential temperature within a layer $\langle \bar{\theta}_z \rangle$, where the angle brackets denote an average over all profiles, to characterize each layer (i.e., cluster) as follows. First, a cluster is identified by visual inspection of the $\theta - S$ diagram. For all profiles that form a particular cluster we compute the vertical temperature gradient within the relevant layer, $\bar{\theta}_z$, and then average over all profiles.

In the DC staircase portion of the water column, $\langle \bar{\theta}_z \rangle$ is close to 0 but can be weakly negative due to the limited resolution of ITP measurements so that $\langle \bar{\theta}_z \rangle \lesssim 0$ (z is defined to be positive upward, Figure 3a). In the deeper region, where intrusions dominate, $\langle \bar{\theta}_z \rangle > 0$ corresponding to the SF stratification within an intrusion. We further introduce the lateral density ratio $R_L = \beta S_L / \alpha \theta_L$ to quantify the relative importance of temperature and salinity variations on density along the layer (subscript L denotes the gradient along

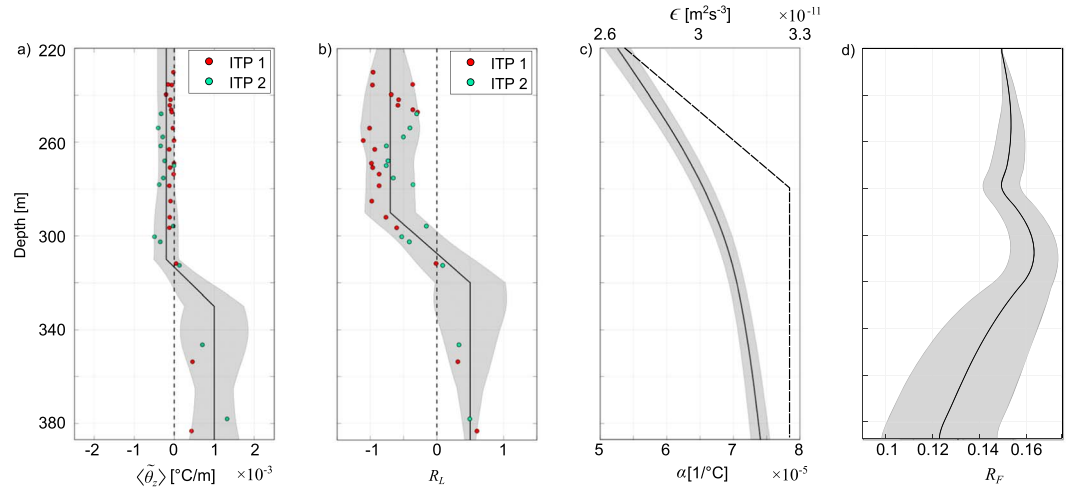


Figure 3. Vertical profiles showing averaged (a) fine-scale vertical gradient $\langle \bar{\theta}_z \rangle$, (b) lateral density ratio R_L , (c) thermal expansion coefficient α (solid line) and the dissipation of turbulent kinetic energy ϵ (dashed line), and (d) vertical flux ratio R_F computed using the bulk formalism. Gray shadings in (a) and (b) denote the uncertainty range as the variance between the piecewise linear fits and point estimates (from ITP 1 and ITP 2) on a 3-m depth grid. Gray shading for α in (c) shows the standard deviation estimated using all profiles (both ITP 1 and ITP 2) and in (d) the error propagation in the integration of (7). ITP = Ice-Tethered Profiler.

the layer). Here $\alpha = -(1/\rho_0)(\partial\rho/\partial\theta)_{s,p}$ is the thermal expansion coefficient and $\beta = (1/\rho_0)(\partial\rho/\partial S)_{\theta,p}$ is the saline contraction coefficient, where ρ_0 is a reference density and p is pressure. R_L is the inverse cluster slope normalized by β/α . In the depth portion where a staircase is observed $R_L < 0$, while $R_L > 0$ in the deeper portion where intrusions are observed (Figure 3b). The transition in depth where $\langle \bar{\theta}_z \rangle$ changes sign generally agrees with the transition from negative to positive R_L (Figures 3a and 3b).

ITP observations suggest that the along-layer property gradients vary with depth as the double-diffusive structures, and associated vertical heat and salt fluxes, change (i.e., transition from staircases to intrusions). Next, using a theoretical approach, we establish a relationship between the depth variation in along-layer gradients and the ratio of vertical heat and salt fluxes through this double-diffusive system.

3. Theoretical Formulation

The general circulation in the Canada Basin is such that the relatively warm saline AW boundary current enters the basin on the western side and cools as it propagates cyclonically around the basin (e.g., Dosser & Timmermans, 2018; Rudels et al., 2013; Woodgate et al., 2007). AW heat and salt are transported laterally from the boundaries into the central basin (approximately from west to east) by the double-diffusive processes driving lateral propagation of thermohaline intrusions. A reasonable assumption is that of a quasi steady state balance with a supply of relatively warm, salty water in the west and cooler, fresher water in the east (albeit marked by occasional pulses of warmer water; McLaughlin et al., 2009; Polyakov et al., 2004). We consider a layer in this steady state balance with double-diffusive mixing as the only mixing process. Assuming that vertical velocity through the double-diffusive system is either 0 or vertically uniform, the advection of properties along the layer is balanced by the vertical divergences of vertical heat flux F_θ and vertical salt flux F_S (see McDougall, 1991), represented as follows:

$$u\theta_L = -F_{\theta_z}, \quad (1)$$

$$uS_L = -F_{S_z}, \quad (2)$$

where u is horizontal velocity along the layer and subscript z denotes vertical derivative. This system can be combined to yield a single equation

$$R_L = \frac{\beta F_{S_z}}{\alpha F_{\theta_z}}. \quad (3)$$

We aim to analyze (3) by relating variations in R_L to variations in F_θ and F_S .

Estimates of heat and salt fluxes can be made by considering the steady state energy balance for a layer (e.g., Hieronymus & Carpenter, 2016):

$$\epsilon = g\alpha F_\theta - g\beta F_S, \quad (4)$$

which relates the dissipation of turbulent kinetic energy ϵ within a layer and the net buoyancy flux for large Rayleigh numbers (Rayleigh numbers are $\gtrsim 10^8$ for the Canada Basin layers; Shibley et al., 2017). Note that (4) assumes that there is no large-scale background shear which is a reasonable assumption given that the lateral density gradient in the Canada Basin at these depths is effectively 0. Moreover, shear-driven mixing due to breaking internal waves is intermittent and weak in the depth region where well-formed staircases and intrusions are present (see Padman & Dillon, 1989) and is neglected in the balance (4). Using (4) and introducing the flux ratio $R_F = \beta F_S / \alpha F_\theta$ (the ratio of the density flux of salt to the density flux of heat), we obtain

$$F_\theta = \frac{\epsilon}{g\alpha(1 - R_F)}, \quad (5)$$

$$F_S = \frac{\epsilon R_F}{g\beta(1 - R_F)}. \quad (6)$$

The balance (4) holds for $R_F < 1$ (so that $\epsilon > 0$ and specifying $F_\theta > 0$ for consistency with the bulk thermal stratification), such that there is a net upward buoyancy flux through the system (here upward fluxes are defined as positive and downward fluxes as negative).

The formalism described here considers an individual layer. It may be equivalently viewed in a bulk sense where, for example, $R_L(z)$ is a continuous representation of the cluster slope changing with depth (Figure 3b). Here we employ this formalism and consider bulk parameters of the Canada Basin double-diffusive system to explain the depth variation of along-layer properties. This avoids the need for data of sufficiently fine resolution to compute fluxes through individual interfaces across the basin scales considered here (see also McDougall, 1991, who uses a smooth Gaussian profile to characterize fluxes through a salt-finger staircase).

Substituting (5) and (6) into (3) yields a differential equation for R_F :

$$R_{Fz} = (R_F - 1) \left[\frac{\alpha_z}{\alpha} \frac{R_L}{1 - R_L} - \frac{\epsilon_z}{\epsilon} \frac{R_L - R_F}{1 - R_L} \right]. \quad (7)$$

In deriving this expression, we have assumed that ϵ weakly varies with depth (this will be discussed in the next section) and used $\beta_z/\beta \ll \alpha_z/\alpha$. In the next section we solve (7) numerically using observations of R_L to obtain a vertical profile of R_F . In Section 5, we interpret the result in context with the physical processes in the double-diffusive system.

4. Context With Observations

We use ITP observations to compute the coefficients in (7) considering the depth range between a shallow bound of the AW layer (around 220-m depth) and the AW temperature maximum around 385-m depth. First, we perform cubic spline smoothing to filter out the fine-scale structures (i.e., staircase and intrusions) in the profiles while retaining the large-scale structure (Figures 1a and 1b). We then use these smoothed profiles of θ and S to compute α (Figure 3c) and α_z . To estimate R_L , we use the simplest piecewise linear profile that approximates the observations from two different ITP systems (Figure 3b). A boundary condition is required for the numerical integration of (7). In the shallow region of the Canada Basin (around ~ 220 m) a well-defined DC staircase is observed (e.g., Padman & Dillon, 1987; Timmermans et al., 2008). In the absence of background shear, vertical heat and salt fluxes are solely due to diffusive convection. For a DC interface separating two well-mixed layers, it has been shown empirically by Turner (1965) that $R_F = 0.15$ if the density ratio across the interface $R_\rho = \beta\delta S/\alpha\delta\theta$ exceeds 2 (here $\delta\theta$ and δS are temperature and salinity differences across the interface). At the top of the domain of interest (220 m) R_ρ ranges between 2 and 7 (e.g., Timmermans et al., 2008), and staircase interfaces are purely DC convection. We therefore take $R_F = 0.15$ as a top boundary condition at 220 m. The integration of (7) requires an estimate for the vertical structure of ϵ over the depth region of interest.

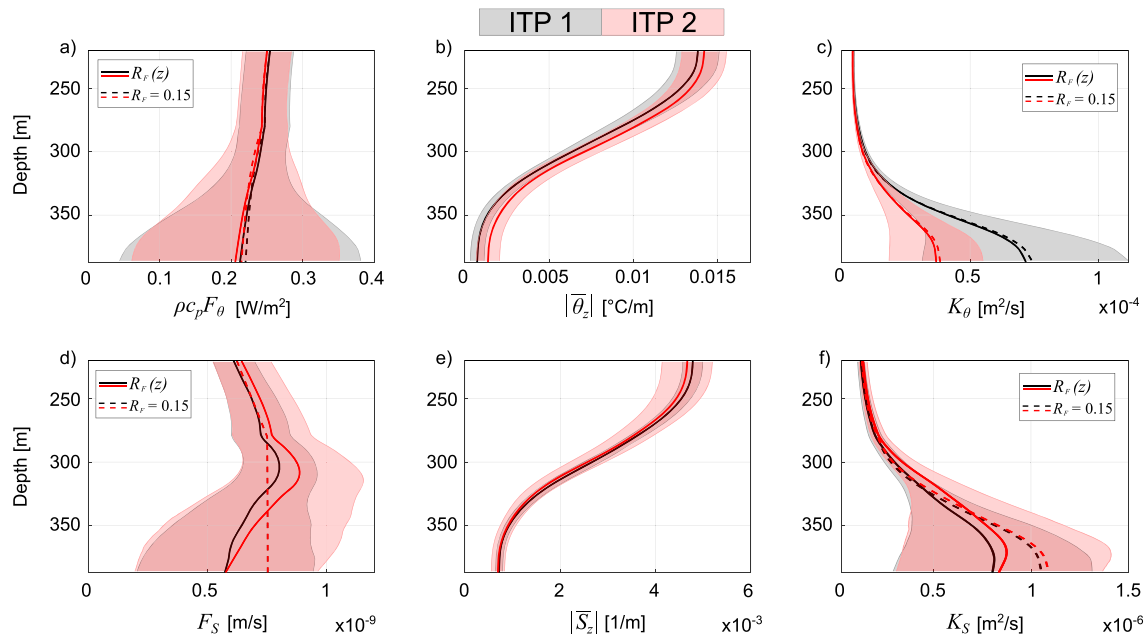


Figure 4. Profiles of (a) vertical heat flux $\rho c_p F_\theta$, (b) absolute value of bulk vertical potential temperature gradient $|\overline{\theta}_z|$, (c) effective diffusivity for heat K_θ , (d) vertical salt flux F_S , (e) absolute value of bulk vertical salinity gradient $|\overline{S}_z|$, and (f) effective diffusivity for salt K_S . The mean of all profiles for ITP 1 are shown in black and for ITP 2 in red. Shadings of the respective color denote one standard deviation from all profiles (panels b and e), and error propagation in the integration of (7) (panels a, c, d, and f). Note that the black dashed line in (d) effectively underlies the red dashed line, which is why it is not visible. ITP = Ice-Tethered Profiler.

In the Arctic Ocean's AW layer, estimated values of ϵ vary by an order of magnitude depending on the region and depth (Lenn et al., 2009; Rainville & Winsor, 2008; Rippeth et al., 2015). In the central Arctic basins away from the boundary regions, however, there is much less spatial variability in ϵ , and observations suggest ϵ varies only weakly over the depth range of the double-diffusive structures (around 220- to 385-m depth, considered here; e.g., Fer, 2009; Guthrie et al., 2015; Lenn et al., 2009). Padman and Dillon (1991) inferred ϵ from microstructure measurements in the Nansen Basin, suggesting that within the depth region of the staircase, ϵ is generally smaller than in the regions where intrusions are present (see their Figure 3). Further, Padman and Dillon (1991) showed that ϵ generally increases as the background stratification decreases and appears to be approximately constant within the AW core where background stratification is weakest. For the numerical integration of (7) we apply the simplest profile of ϵ that is consistent with this general picture of ϵ increasing with depth in the staircase region and remaining constant with depth in the intrusion region (the transition in depth at 280 m is chosen based on the background profile of buoyancy frequency and fine-structure observations discussed in section 5). We take ϵ varying from 2.7×10^{-11} to $\sim 3.3 \times 10^{-11}$ m²/s³ (which is consistent with observations from the central basins; Fer, 2009). This choice can be further justified by comparing the profiles of $\rho c_p F_\theta$ (where ρ is density and c_p is the specific heat of seawater) with heat fluxes of around 0.2 W/m² inferred from observations in the double-diffusive staircase (e.g., Padman & Dillon, 1987; Timmermans et al., 2008); the chosen profile of ϵ in (5) returns heat fluxes of a similar value to those estimated from observations (Figure 4a).

$R_F(z)$ is then computed by integration of (7), with uncertainty estimated through error propagation of uncertainties in the coefficients (see, e.g., Taylor, 1997). $R_F(z) \approx 0.15$ from 220- to ~ 280 -m depth. From ~ 280 - to 310-m depth, R_F increases and subsequently decreases to 385-m depth (Figure 3d). This implies that the effect of the salt flux on density flux becomes relatively larger with depth compared to the effect of the heat flux from 280 to ~ 310 m, and then the opposite is true with further increases in depth. Flux profiles indicate that the vertical structure of R_F relates predominantly to the depth variation of the salt flux which reaches a maximum at around 310 m and decreases with depth thereafter (Figure 4d). By comparison, the heat flux changes relatively little with depth and shows a monotonic decrease (Figure 4a). Note, however, that this

vertical structure of R_F is sensitive to the exact profile chosen for ϵ with weaker vertical variation in ϵ in the shallow region resulting in a shallower transition depth from $R_F = 0.15$ to the larger values.

In sum, the depth variation of R_F explains the observed depth variation in R_L (i.e., along-layer temperature and salinity gradients), and furthermore, depth variations in R_F are dominated by salinity flux divergences. We conclude that salinity increases from west to east along layers at shallow depths and decreases from west to east at deeper levels because the vertical salt flux divergence changes sign with depth (Figure 4d). Temperature decreases from west to east along layers at all depths because vertical heat flux divergence does not change sign with depth.

If the flux ratio were constant in the system, say $R_F = \beta F_S / \alpha F_\theta = 0.15$, then from (4), αF_θ should be constant within the depth region of the intrusions where ϵ does not vary with depth. Thus, βF_S must also be constant. The saline contraction coefficient β varies by less than 1% over this depth range, which would imply a vertical salt flux that is effectively constant with depth ($F_{S_z} \approx 0$; Figure 4d) as would be the slope of clusters in $\theta - S$ space (salinity would be constant along each layer). Therefore, the observations (i.e., cluster slopes) are not consistent with R_F being constant with depth.

Finally, we note that heat and salt fluxes can be expressed in terms of effective vertical diffusivities for heat (K_θ) and salt (K_S) as

$$F_\theta = -K_\theta \bar{\theta}_z, \quad (8)$$

$$F_S = -K_S \bar{S}_z, \quad (9)$$

where the overbar denotes a bulk gradient (i.e., estimated on a scale that is larger than an individual layer). This yields an estimated range of K_θ that agrees well with estimates of K_θ from measurements which vary between 10^{-6} and 10^{-4} m²/s (e.g., Guthrie et al., 2013; Sirevaag & Fer, 2012) in the depth region of double-diffusive structures. K_S also takes a reasonable range of values (Figure 4f) in the staircase region (see Bebieva & Timmermans, 2016).

Thus far, we have considered a bulk formalism to show how the depth-varying along-layer $\theta - S$ gradients are consistent with a ratio of fluxes changing with depth in the region of double-diffusive structures, including staircases and intrusions. This result leads naturally to the following questions: How does the ratio of fluxes relate to particular types of double-diffusive structures? What sets the depth range over which different double-diffusive structures persist? To address these questions, we must return to an analysis that considers individual double-diffusive layers and the fine-scale structures within the layers and at the interfaces.

5. Interpreting the Vertical Structure of the Flux Ratio, R_F

In a water column that is unstable to double diffusion, the motion is driven by the release of potential energy of the density component that is unstably stratified. If stratification is DC-amenable, then both heat (F_θ^{DC}) and salt (F_S^{DC}) fluxes are upward. The flux ratio in this case is $R_F^{\text{DC}} = \beta F_S^{\text{DC}} / \alpha F_\theta^{\text{DC}} = 0.15$, which applies for $R_\rho > 2$ (Sommer et al., 2014; Turner, 1965). For the SF-amenable stratification, both heat (F_θ^{SF}) and salt (F_S^{SF}) fluxes are downward, and the vertical flux ratio is given by

$$\gamma = \alpha F_\theta^{\text{SF}} / \beta F_S^{\text{SF}} < 1. \quad (10)$$

In a water column where the layers are bounded in depth by both DC and SF regions, we can write the net flux ratio as

$$R_F = \frac{\beta F_S}{\alpha F_\theta} = \frac{\beta(|F_S^{\text{DC}}| - |F_S^{\text{SF}}|)}{\alpha(|F_\theta^{\text{DC}}| - |F_\theta^{\text{SF}}|)}. \quad (11)$$

Here the directions of fluxes are taken into account (upward fluxes are positive), and we assume that net fluxes (F_S and F_θ) are upward which is necessary for consistency with the bulk results (Figure 4, where the heat and salt fluxes are derived from (5) and (6)). Guided by the fine-scale ITP observations, we have

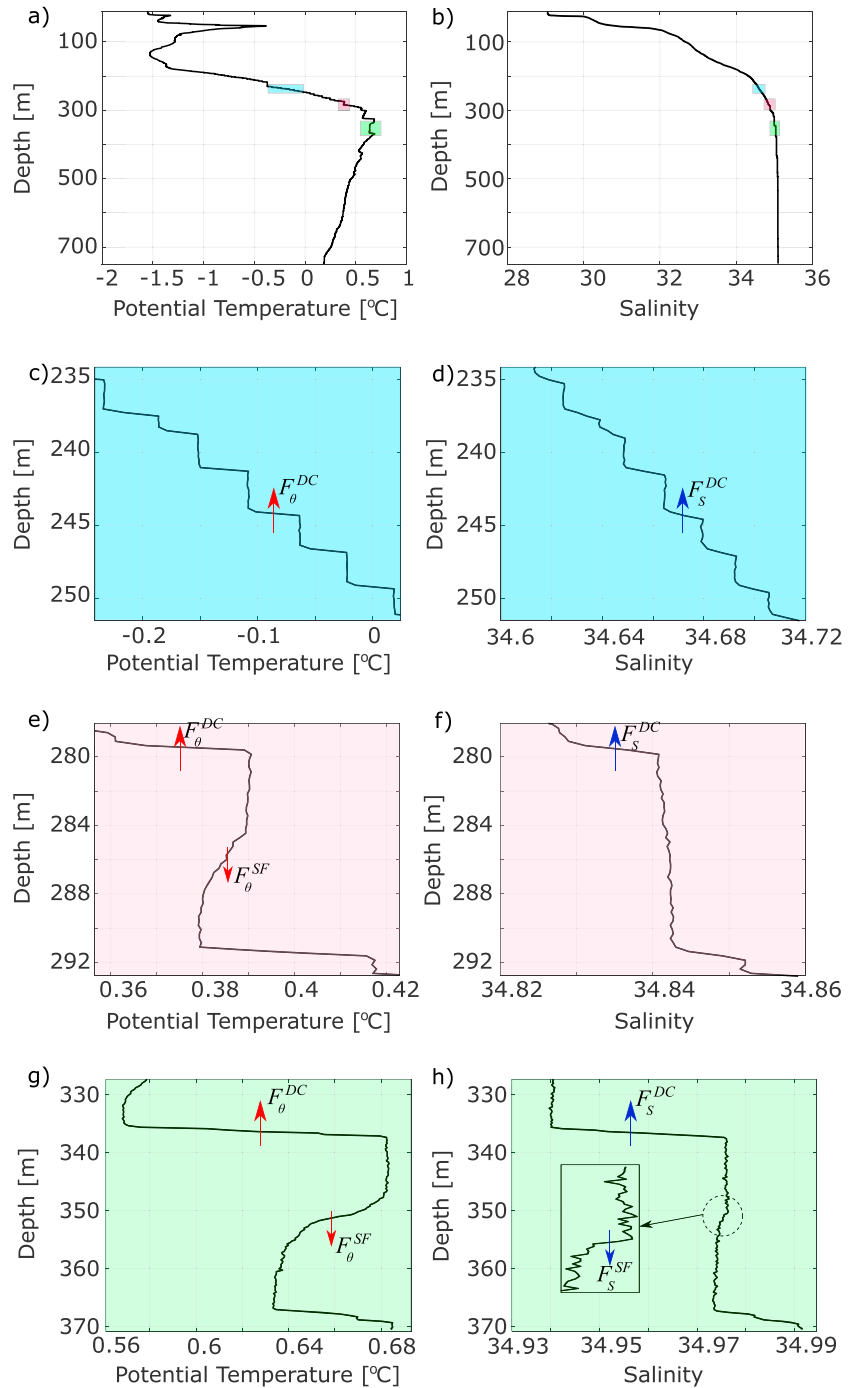


Figure 5. Typical (a) potential temperature ($^{\circ}\text{C}$, referenced to the surface) and (b) salinity profiles measured by ITP 2. The expanded scales in panels (e)–(h) correspond to the colored shadings in (a) and (b) showing three depth regions identified in section 5: (c and d) the double-diffusive staircase; (e and f) remnant intrusions; and (g and h) active intrusions. The arrows show the directions of heat (F_{θ} , in red) and salt (F_S , in blue) fluxes, and superscripts DC and SF represent fluxes due to diffusive convection and salt fingers, respectively. ITP = Ice-Tethered Profiler.

identified three distinct regions with respect to double diffusion within the upper portion of the AW layer (Figures 5a and 5b):

- (I) *Double-diffusive staircase*. The shallowest depth region, between around 220- and 280-m depth, exhibits only DC interfaces and mixed layers (Figures 5c and 5d). Therefore, heat and salt are fluxed only upward.
- (II) *Remnant intrusions*. In this depth region (\sim 280- to 320-m depth) ITP data show inversions in temperature profiles in place of well-mixed layers. Salinity profiles, on the other hand, show either a well-mixed layer or a weak negative gradient (i.e., salinity increases with depth within the layer; Figures 5e and 5f). These temperature and salinity gradients are well resolved in the ITP data and observed in nearly 50% of all profiles analyzed.

We hypothesize that this structure originates from an intrusion and refer to it as a *remnant intrusion*. Expressing SF salt and heat fluxes in terms of effective diffusivities (K_S^{SF} and K_θ^{SF}) and gradients (i.e., similar to (8)–(9)) yields $K_S^{\text{SF}}/K_\theta^{\text{SF}} > 1$ (recall that $\gamma < 1$ and the temperature effect on buoyancy is less than the salinity effect on buoyancy in this SF region)). The larger K_S^{SF} compared to K_θ^{SF} suggests that a scenario can arise where an SF portion of an intrusion characterized by S and θ decreasing with depth can “run down” the salt gradient faster than the temperature gradient. Numerical studies of two-layer SF-stratified systems also show that over time the salinity gradient tends to 0, while the temperature gradient remains finite (e.g., Singh & Srinivasan, 2014). Moreover, Traxler et al. (2011) performed numerical simulations of salt fingering and found that γ varies from 0.63 to 0.46 and $K_S^{\text{SF}}/K_\theta^{\text{SF}} \approx 2$ –20. In this depth region of remnant intrusions, heat is fluxed in both directions: upward through a DC interface and downward into the deeper region through the SF remnant portion of intrusions, while salt is only fluxed upward through a DC interface (Figures 5e and 5f).

- (III) *Active intrusions*. In the deepest region (\sim 320- to 385-m depth), thermohaline intrusions are active and characterized by conventional DC- and SF-stratified regions alternating in depth. Associated heat and salt fluxes are upward in the DC region and downward in the SF region (Figures 5g and 5h). Intrusions are thought to advect laterally because the vertical flux divergences associated with both SF and DC fluxes lead to a net buoyancy change (Li & McDougall, 2015); this is consistent with clusters crossing isopycnals in $\theta - S$ space (i.e., a layer is denser in the east compared to that in the west, Figure 2).

For each of these three depth regions we consider net upward heat and salt fluxes in terms of DC and SF flux components and estimate the net R_F from (11). In the staircase region (I), vertical fluxes are only due to DC mixing. Based on the laboratory results of Turner (1965), and given that $R_\rho > 2$, it is expected that $R_F \approx 0.15$ in region (I).

In the depth region of remnant intrusions (II), $F_S^{\text{SF}} = 0$ because the salinity gradient has run down ($S_z = 0$). F_θ^{SF} is computed as proportional to the temperature gradient within a layer (a typical value is $\theta_z^{\text{SF}} \approx 0.0025$ °C/m, Figure 5e) and taking K_θ^{SF} to be in the range of $0.47 - 21 \times 10^{-6}$ m²/s (see Traxler et al., 2011). F_θ^{DC} may be computed using the 4/3-flux law (Kelley, 1990), which is based on the difference in temperature across a DC interface (having typical value ≈ 0.04 °C). F_S^{DC} is then known given the constant $R_F^{\text{DC}} = 0.15$. Further within the uncertainty range for K_θ^{SF} , R_F may take values within the range [0.15;1], where the upper bound is set to be 1 for consistency with the bulk formalism.

In the region of active intrusions (III), we may obtain bounds on fluxes and R_F , by first rewriting (11) as

$$R_F = 0.15 \frac{1 - |F_S^{\text{SF}}|/|F_S^{\text{DC}}|}{1 - 0.15\gamma|F_S^{\text{SF}}|/|F_S^{\text{DC}}|}. \quad (12)$$

For consistency with the bulk formalism indicating net positive salt flux, $|F_S^{\text{SF}}|/|F_S^{\text{DC}}| < 1$. Together with the estimated range of γ (0.46 – 0.63; Traxler et al., 2011), this yields $R_F < 0.15$. We deduce that after R_F increases with depth in the region of remnant intrusions (II), it then decreases with depth toward 0.15 and possibly smaller where active intrusions persist. This structure of R_F inferred from the fine-scale measurements agrees qualitatively with the structure inferred from the bulk formalism and observed depth variation of R_L . The discrepancies between these two approaches might appear because of the inherent limitation of the bulk formalism (that uses smoothed profiles) to capture fine-scale processes at the interfaces of the layers.

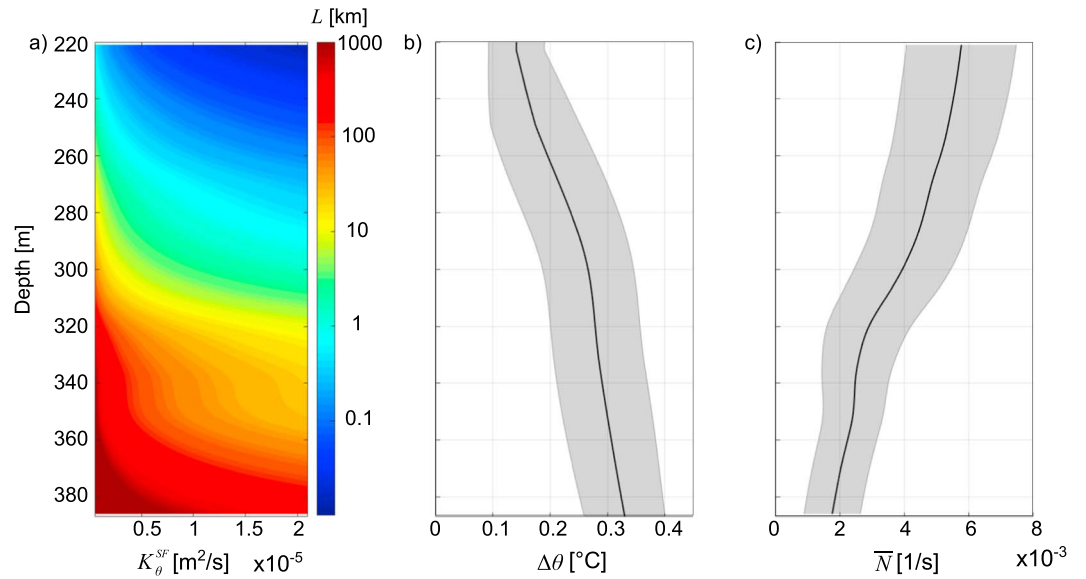


Figure 6. (a) The distance L (km) that intrusions propagate before they fully run down (color) as a function of depth and vertical SF heat diffusivity K_{θ}^{SF} (m^2/s). Calculations use the mean profile (over all ITP 1 and ITP 2 profiles combined) of (b) maximum lateral potential temperature difference $\Delta\theta$ ($^{\circ}C$) and (c) background buoyancy frequency \bar{N} ($1/s$). Gray shadings denote one standard deviation. ITP = Ice-Tethered Profiler; SF = salt finger.

6. Factors Controlling the Transition From Staircase to Intrusions

While we have shown how the vertical structure of R_F , which can explain the observed vertical structure of R_L , is consistent with the fine-scale double-diffusive structures, the factors that set the depth at which the staircase structure transitions to intrusions remains to be understood. To explore this depth dependence, we begin with the hypothesis that a staircase can be viewed as the run-down state of thermohaline intrusions.

We assume that SF fluxes dominate the rundown of SF gradients. Further, as noted above, the temperature gradient remains after the salinity gradient has already run down (since $K_S^{SF}/K_{\theta}^{SF} \approx 2-20$; Traxler et al., 2011). Therefore, thermohaline intrusions have fully run down to staircases on the diffusive time scale given by $\tau \sim H^2/K_{\theta}^{SF}$, where H is the vertical scale of an SF portion of an intrusion. To estimate the distance $L = U\tau$ that intrusions can propagate before fully transitioning to a staircase, we require an estimate of their lateral propagation velocity U . The speed of intrusions can be approximated as $U = C\bar{N}H$ (Kerr, 2007; Manins, 1976; Maurer et al., 2010), where C is a constant and \bar{N} is the background buoyancy frequency in the region into which intrusions propagate ($\bar{N} = \sqrt{-g\rho_z/\rho_0}$ may be computed from the smoothed temperature and salinity profiles, where $\rho = \rho(\theta, S)$, assuming that intrusions do not alter the large-scale vertical stratification significantly). This formulation is similar to that characterizing the nose velocity of gravity currents in continuously stratified fluids and can be derived from energy conversion arguments where the mean potential energy of a fluid system is converted to kinetic energy (Turner, 1973). For gravity currents $C = O(1)$; however, for thermohaline intrusions this constant is likely to be much smaller: Laboratory studies by Ruddick et al. (1999) suggest $C = 0.005$, while numerical simulations by Simeonov and Stern (2007) suggest $C = 0.14$. Also, based on laboratory experiments and energetics, the vertical scale of thermohaline intrusions may be estimated as $H = g\alpha\Delta\theta/\bar{N}$, where $\Delta\theta$ is a lateral temperature difference ($\beta\Delta S$ could be equivalently used in place of $\alpha\Delta\theta$ assuming density compensating lateral gradients; Chen et al., 1971; Ruddick & Turner, 1979). Here we estimate $\Delta\theta$ as the east-west difference over the region sampled by the ITPs between maximum and minimum temperatures recorded at a given depth (i.e., the end-member temperatures).

The above formulations of run-down time scale τ , intrusion propagation velocity U and vertical scale H yield

$$L = U\tau = C \frac{(g\alpha\Delta\theta)^3}{\bar{N}^5 K_{\theta}^{SF}}. \quad (13)$$

We take $C = 0.005$ as it gives $U = O(1)$ mm/s, which is comparable to intrusion speeds estimated based on two different surveys through the same intrusions in the eastern Atlantic Ocean (Ruddick & Hebert, 1988). The higher value of $C = 0.14$ was estimated based on numerical experiments considering an SF unstable background stratification (Simeonov & Stern, 2007) and may not be relevant for this case. For the Canada Basin's parameter range, order of magnitude computations suggest that intrusions can travel for several kilometers in the shallow portion to hundreds of kilometers in the deeper portion before they fully run down (Figure 6a). The dominant factors in setting this distance are background stratification and lateral temperature difference with SF vertical diffusivity of heat playing a smaller role. Stronger stratification and weaker $\Delta\theta$ in the shallow portion of the water column limit lateral propagation of the intrusions, while weaker stratification and larger $\Delta\theta$ in the deeper portion allow intrusions to propagate much longer distances before running down to a staircase (Figures 6b and 6c). Note that in the slant-wise convection description of intrusions, convective cells become increasingly vertical during the run-down process (Walsh & Carmack, 2003, their Figure 10).

Uncertainties in \bar{N} and $\Delta\theta$ (Figures 6b and 6c) yield L estimates that differ by about a factor of 2 in the shallow region and a factor of 5 in the deeper region. While we have chosen a value of C that gives propagation velocities consistent with other estimates for ocean intrusions, this free parameter is an additional source of uncertainty. Moreover, this simple model assumes that intrusions spread eastward from the western boundary into the central basin and that the ITP drift region covers the full range of lateral temperature gradients. The effect of DC fluxes on dissipation of SF gradients within intrusions may affect these calculations as well. Nevertheless, estimates of L are in broad agreement with the hypothesis of a transition in depth from staircases to intrusions that depends upon the lateral background gradient and vertical stratification. In sum, the distance L that intrusions can travel before running down to staircases varies with depth as a function of $\Delta\theta$ and \bar{N} . Shorter L relates to the shallower staircases, while longer L supports the intrusion structures further into the basin. The transition from shorter to longer L corresponds to the depth of transition from staircases to remnant and active intrusions.

Finally, we note that the analysis above suggests the expectation that the slope of clusters in $\theta - S$ space would evolve as intrusions run down. However, ITPs drift across the basin making profiles on time scales much faster than the evolution time scales of the intrusions (we estimate that SF gradients would fully run down in years to decades), and it is not possible to track the evolution of an individual cluster slope in $\theta - S$ space.

7. Summary and Discussion

We have examined the depth variation of temperature and salinity gradients along Canada Basin staircase mixed layers and intrusive layers whose properties form clusters in $\theta - S$ space. The cluster slopes change with depth in response to the varying ratio of net vertical salt to heat fluxes which depends on the interplay between DC and SF fluxes in a given layer (i.e., whether a layer is part of a staircase or intrusion).

Our analysis suggests that a staircase may be formed by the rundown of thermohaline intrusions. Scaling indicates that the distance intrusions can propagate before running down depends predominantly on the vertical stratification and the lateral background buoyancy gradient arising from the temperature difference (or equivalently the salinity difference). Our estimates that intrusions in the deeper portions of the water column can travel hundreds of kilometers before they transition to a staircase, and only several kilometers in the shallow portion, are consistent with observations showing a staircase in the shallower depths and intrusions at deeper levels. We remark that this finding further implies that effective lateral diffusivities (and therefore lateral heat and salt transport) are not only functions of depth but also depend strongly on lateral position in the basin with respect to the AW boundary current.

This study contributes to previous studies that have suggested staircase structures are related to intrusions (Bebieva & Timmermans, 2017; Merryfield, 2000; Walsh & Carmack, 2002). Bebieva and Timmermans (2017) showed that either staircases or intrusions can emerge as the result of a perturbation to a background linear vertical stratification in the presence of lateral property gradients. The scenario of intrusions emerging is not inconsistent with the analysis presented here; intrusions develop and then run down to form a staircase. In our analysis here, we have estimated that intrusions may only travel a few kilometers before running down at shallow depths in the Canada Basin (i.e., intrusions at these shallow depths would only be observed in the immediate vicinity of the AW boundary current). This must be reconciled with the

observation that staircases are observed across the entire Canada Basin, for hundreds of kilometers east of the AW boundary current, with individual layers being laterally coherent for these distances. Could it be that these staircases, observed far from the western boundary, are the manifestation of instability of the background temperature and salinity stratification? How then do they relate to intrusions (emerging near the boundary) that have run down?

Perhaps one way to envision the Canada Basin double-diffusive system is by considering the anomalously warm and salty AW influx to the Canada Basin conceptually as a laboratory tank lock exchange problem. In this configuration, a vertical barrier separates two reservoirs containing stratified fluid with lateral jumps in θ and S across the barrier that are density compensating at each depth. Upon removal of the barrier, intrusions are observed at all depths (e.g., see Ruddick et al., 1999). According to our hypothesis here, intrusions emerging from the front (representing the AW boundary current along the Canada Basin's western boundary) spread laterally and eventually run down to staircases. The scenario is further complicated by the fact that intrusions are likely advected laterally by the background geostrophic flow in the basin (see, e.g., McLaughlin et al., 2009). It may be that staircases in the central basin form as the result of a wave-like perturbation originating from the upstream intrusions at those depths (Bebieva & Timmermans, 2017). Laboratory lock exchange experiments, for example, indicate velocity perturbations attributed to internal gravity waves far beyond the intrusion front (Ruddick et al., 1999). Staircases emerging from such perturbations may be consistent with the lateral coherence of layers from the basin boundary to the interior, although the relationship is highly speculative. More detailed analyses are needed to better understand intrusion/staircase links. Further, the details of the run-down process require investigation, and our results highlight the ongoing need for additional field observations spanning the vast range of temporal and spatial scales of relevance to these double-diffusive structures.

Acknowledgments

The Ice-Tethered Profiler data were collected and made available by the Ice-Tethered Profiler Program based at the Woods Hole Oceanographic Institution (Krishfield et al., 2008; Toole et al., 2011); data are available at <http://www.whoi.edu/itp/data>. Funding was provided by the National Science Foundation Division of Polar Programs under award 1350046. We thank Laurie Padman and an anonymous reviewer for their constructive and thoughtful reviews. We acknowledge support and valuable discussions during the Forum for Arctic Modeling and Observational Synthesis (FAMOS) and the associated FAMOS School.

References

- Bebieva, Y., & Timmermans, M.-L. (2016). An examination of double-diffusive processes in a mesoscale eddy in the Arctic Ocean. *Journal of Geophysical Research: Oceans*, *121*, 457–475. <https://doi.org/10.1002/2015JC011105>
- Bebieva, Y., & Timmermans, M.-L. (2017). The relationship between double-diffusive intrusions and staircases in the Arctic Ocean. *Journal of Physical Oceanography*, *47*(4), 867–878.
- Carmack, E. C., Aagaard, K., Swift, J. H., Perkin, R. G., McLaughlin, F., Macdonald, R., & Jones, E. (1998). Thermohaline transitions. In J. Imberger (Ed.), *Physical processes in lakes and oceans* (pp. 179–186). Washington, DC: American Geophysical Union.
- Chen, C., Briggs, D., & Wirtz, R. (1971). Stability of thermal convection in a salinity gradient due to lateral heating. *International Journal of Heat and Mass Transfer*, *14*(1), 57–65.
- Dosser, H., & Timmermans, M.-L. (2018). Inferring circulation and lateral eddy fluxes in the Arctic Oceans deep Canada Basin using an inverse method. *Journal of Physical Oceanography*, *48*(2), 245–260.
- Fer, I. (2009). Weak vertical diffusion allows maintenance of cold halocline in the central Arctic. *Atmospheric and Oceanic Science Letters*, *2*(3), 148–152.
- Guthrie, J. D., Fer, I., & Morison, J. (2015). Observational validation of the diffusive convection flux laws in the Amundsen Basin, Arctic Ocean. *Journal of Geophysical Research: Oceans*, *120*, 7880–7896. <https://doi.org/10.1002/2015JC010884>
- Guthrie, J. D., Morison, J. H., & Fer, I. (2013). Revisiting internal waves and mixing in the Arctic Ocean. *Journal of Geophysical Research: Oceans*, *118*, 3966–3977. <https://doi.org/10.1002/jgrc.20294>
- Hieronimus, M., & Carpenter, J. R. (2016). Energy and variance budgets of a diffusive staircase with implications for heat flux scaling. *Journal of Physical Oceanography*, *46*(8), 2553–2569.
- Kelley, D. E. (1990). Fluxes through diffusive staircases: A new formulation. *Journal of Geophysical Research*, *95*(C3), 3365–3371.
- Kerr, O. S. (2007). Periodic intrusions in a stratified fluid. *Journal of Fluid Mechanics*, *580*, 467–480.
- Krishfield, R., Toole, J., Proshutinsky, A., & Timmermans, M.-L. (2008). Automated ice-tethered profilers for seawater observations under pack ice in all seasons. *Journal of Atmospheric and Oceanic Technology*, *25*(11), 2091–2105.
- Lenn, Y.-D., Wiles, P., Torres-Valdes, S., Abrahamsen, E., Rippeth, T., Simpson, J., et al. (2009). Vertical mixing at intermediate depths in the Arctic boundary current. *Geophysical Research Letters*, *36*, L05601. <https://doi.org/10.1029/2008GL036792>
- Li, Y., & McDougall, T. J. (2015). Double-diffusive interleaving: Properties of the steady-state solution. *Journal of Physical Oceanography*, *45*(3), 813–835.
- Manins, P. (1976). Intrusion into a stratified fluid. *Journal of Fluid Mechanics*, *74*(3), 547–560.
- Maurer, B. D., Bolster, D. T., & Linden, P. (2010). Intrusive gravity currents between two stably stratified fluids. *Journal of Fluid Mechanics*, *647*, 53–69.
- McDougall, T. J. (1991). Interfacial advection in the thermohaline staircase east of Barbados. *Deep Sea Research Part A: Oceanographic Research Papers*, *38*(3), 357–370.
- McLaughlin, F., Carmack, E., Macdonald, R., Melling, H., Swift, J., Wheeler, P., et al. (2004). The joint roles of Pacific and Atlantic-origin waters in the Canada Basin, 1997–1998. *Deep Sea Research Part 1: Oceanographic Research Papers*, *51*(1), 107–128. <https://doi.org/10.1016/j.dsr.2003.09.010>
- McLaughlin, F., Carmack, E., Williams, W., Zimmermann, S., Shimada, K., & Itoh, M. (2009). Joint effects of boundary currents and thermohaline intrusions on the warming of Atlantic water in the Canada Basin, 1993–2007. *Journal of Geophysical Research*, *114*, C00A12. <https://doi.org/10.1029/2008JC005001>
- Merryfield, W. J. (2000). Origin of thermohaline staircases. *Journal Physical Oceanography*, *30*(5), 1046–1068.
- Neal, V. T., & Neslyba, S. (1973). Microstructure anomalies in the Arctic Ocean. *Journal of Geophysical Research*, *78*(15), 2695–2701.

- Neshyba, S., Neal, V. T., & Denner, W. (1971). Temperature and conductivity measurements under Ice Island T-3. *Journal of Geophysical Research*, 76(33), 8107–8120.
- Padman, L., & Dillon, T. M. (1987). Vertical heat fluxes through the Beaufort Sea thermohaline staircase. *Journal of Geophysical Research*, 92(C10), 10,799–10,806.
- Padman, L., & Dillon, T. M. (1989). Thermal microstructure and internal waves in the Canada Basin diffusive staircase. *Deep Sea Research Part A. Oceanographic Research Papers*, 36(4), 531–542.
- Padman, L., & Dillon, T. M. (1991). Turbulent mixing near the Yermak Plateau during the Coordinated Eastern Arctic Experiment. *Journal of Geophysical Research*, 96(C3), 4769–4782.
- Perkin, R., & Lewis, E. (1984). Mixing in the West Spitsbergen Current. *Journal of Physical Oceanography*, 14(8), 1315–1325.
- Polyakov, I., Alekseev, G., Timokhov, L., Bhatt, U., Colony, R., Simmons, H., et al. (2004). Variability of the intermediate Atlantic water of the Arctic Ocean over the last 100 years. *Journal of Climate*, 17(23), 4485–4497.
- Rainville, L., & Winsor, P. (2008). Mixing across the Arctic Ocean: Microstructure observations during the Beringia 2005 expedition. *Geophysical Research Letters*, 35, L08606. <https://doi.org/10.1029/2008GL033532>
- Rippeth, T. P., Lincoln, B. J., Lenn, Y.-D., Green, J. M., Sundfjord, A., & Bacon, S. (2015). Tide-mediated warming of Arctic halocline by Atlantic heat fluxes over rough topography. *Nature Geoscience*, 8(3), 191–194.
- Ruddick, B., & Hebert, D. (1988). The mixing of Meddy “Sharon”. *Elsevier Oceanography Series*, 46, 249–261.
- Ruddick, B., Phillips, O. M., & Turner, J. S. (1999). A laboratory and quantitative model of finite-amplitude thermohaline intrusions. *Dynamics of Atmospheres and Oceans*, 30(2), 71–99.
- Ruddick, B., & Turner, J. (1979). The vertical length scale of double-diffusive intrusions. *Deep Sea Research Part A. Oceanographic Research Papers*, 26(8), 903–913.
- Rudels, B., Schauer, U., Björk, G., Korhonen, M., Pisarev, S., Rabe, B., & Wisotzki, A. (2013). Observations of water masses and circulation in the Eurasian Basin of the Arctic Ocean from the 1990s to the late 2000s. *OS Special Issue: Ice-Atmosphere-Ocean Interactions in the Arctic Ocean during IPY: The Damocles Project*, 9(1), 147–169.
- Shibley, N. C., Timmermans, M.-L., Carpenter, J. R., & Toole, J. M. (2017). Spatial variability of the Arctic Ocean's double-diffusive staircase. *Journal of Geophysical Research: Oceans*, 122, 980–994. <https://doi.org/10.1002/2016JC012419>
- Simeonov, J., & Stern, M. E. (2007). Equilibration of two-dimensional double-diffusive intrusions. *Journal of Physical Oceanography*, 37(3), 625–643.
- Singh, O., & Srinivasan, J. (2014). Effect of Rayleigh numbers on the evolution of double-diffusive salt fingers. *Physics of Fluids*, 26(6), 062104.
- Sirevaag, A., & Fer, I. (2012). Vertical heat transfer in the Arctic Ocean: The role of double-diffusive mixing. *Journal of Geophysical Research*, 117, C07010. <https://doi.org/10.1029/2012JC007910>
- Sommer, T., Carpenter, J. R., & Wüest, A. (2014). Double-diffusive interfaces in Lake Kivu reproduced by direct numerical simulations. *Geophysical Research Letters*, 41, 5114–5121. <https://doi.org/10.1002/2014GL060716>
- Taylor, J. R. (1997). *Introduction to error analysis, the study of uncertainties in physical measurements*, A series of books in physics. New York: University Science Books.
- Timmermans, M.-L., Toole, J. M., Krishfield, R., & Winsor, P. (2008). Ice-tethered profiler observations of the double-diffusive staircase in the Canada Basin thermocline. *Journal of Geophysical Research*, 113, C00A02. <https://doi.org/10.1029/2008JC004829>
- Toole, J. M., Krishfield, R. A., Timmermans, M.-L., & Proshutinsky, A. (2011). The ice-tethered profiler: Argo of the Arctic. *Oceanography*, 24(3), 126–135.
- Traxler, A., Stellmach, S., Garaud, P., Radko, T., & Brummell, N. (2011). Dynamics of fingering convection. Part 1 Small-scale fluxes and large-scale instabilities. *Journal of Fluid Mechanics*, 677, 530–553.
- Turner, J. (1965). The coupled turbulent transports of salt and and heat across a sharp density interface. *International Journal of Heat and Mass Transfer*, 8(5), 759–767.
- Turner, J. (1973). *Buoyancy effects in fluids*. London, UK: Cambridge University Press.
- Walsh, D., & Carmack, E. (2002). A note on evanescent behavior of Arctic thermohaline intrusions. *Journal of Marine Research*, 60(2), 281–310.
- Walsh, D., & Carmack, E. (2003). The nested structure of Arctic thermohaline intrusions. *Ocean Modelling*, 5(3), 267–289.
- Woodgate, R. A., Aagaard, K., Swift, J. H., Smethie, W. M., & Falkner, K. K. (2007). Atlantic water circulation over the Mendeleev Ridge and Chukchi Borderland from thermohaline intrusions and water mass properties. *Journal of Geophysical Research*, 112, C02005. <https://doi.org/10.1029/2005JC003416>